

A&A manuscript no.  
(will be inserted by hand later)

Your thesaurus codes are:  
03 (13.25.2;11.19.1;11.09.1: NGC 2992)

# The variability of the Seyfert galaxy NGC 2992: the case for a revived AGN

R. Gilli<sup>1\*</sup>, R. Maiolino<sup>2</sup>, A. Marconi<sup>2</sup>, G. Risaliti<sup>1</sup>, M. Dadina<sup>3</sup>, K.A. Weaver<sup>4</sup>, and E.J.M. Colbert<sup>4</sup>

<sup>1</sup> Dipartimento di Astronomia e Scienza dello Spazio, Università di Firenze, Largo E. Fermi 5, I-50125 Firenze, Italy (gilli, risaliti@arcetri.astro.it)

<sup>2</sup> Osservatorio Astrofisico di Arcetri, Largo E. Fermi 5, I-50125 Firenze, Italy (maiolino, marconi@arcetri.astro.it)

<sup>3</sup> BeppoSAX SDC, ASI, Via Corcolle 19, I-00131 Roma, Italy (dadina@gavi.sdc.asi.it)

<sup>4</sup> Laboratory for High Energy Astrophysics, Code 662, NASA/GSFC, Greenbelt, MD 20771, USA (kweaver, colbert@gsfc.nasa.gov)

Received / Accepted

**Abstract.** We report the transition to an active state of the nucleus in the Seyfert 1.9 galaxy NGC 2992, discovered by means of new hard X-ray data. While the 2–10 keV flux declined by a factor of  $\sim 20$  from 1978 to 1994, two recent BeppoSAX observations in 1997 and in 1998 caught the nuclear emission raising back to the same level of activity observed in 1978.

In both BeppoSAX observations the X-ray spectrum of the source is well represented by a power law with spectral index  $\Gamma \simeq 1.7$ , absorbed by a column density of  $N_{\text{H}} \simeq 10^{22} \text{ cm}^{-2}$  and characterized by a prominent iron  $K\alpha$  line. While in the second BeppoSAX data set the line properties appear to be consistent with those expected from accretion disc models, in the first BeppoSAX data set the iron feature is rather peculiar. The broadening is not significant and the line energy is  $E_{K\alpha} = 6.62 \pm 0.07$  keV, indicating emission from highly ionized iron. The line has too high equivalent width ( $\sim 700$  eV) to be produced by a hot scattering medium. By comparing these data with data previously in the literature, we interpret the spectral and flux changes in terms of different phases of rebuilding an accretion disc. The timescale for the disc rebuilding is estimated to range between 1 and 5 years.

The X-ray data are complemented with optical and near-infrared followup spectra taken 1.5 months after the discovery of the X-ray burst. The spectra are characterized by prominent broad emission lines. There is also evidence for hot dust emission in the H and K bands that, however, is probably still in the process of increasing.

**Key words:** X-rays: galaxies – Galaxies: Seyfert – Galaxies: individual: NGC 2992

*Send offprint requests to:* R. Gilli

\* Present address: Astrophysikalisches Institut Potsdam, An der Sternwarte 16, D-14482 Potsdam, Germany

## 1. Introduction

The Seyfert 1.9 galaxy NGC 2992 is a nearby ( $z=0.0077$ ), edge on ( $i = 70^\circ$ ) system interacting with NGC 2993. The detection of a broad component of  $H\alpha$  with no  $H\beta$  counterpart (Ward et al. 1980; Shuder 1980) implied an intermediate Seyfert type classification, suggesting the existence of an obscured broad line region (BLR). This was confirmed later by the infrared detection of a broad  $\text{Pa}\alpha$  line (Rix et al. 1990; Goodrich, Veilleux & Hill 1994). The optical image of NGC 2992 (Ward et al. 1980) shows a prominent dust lane extending along the major axis of the galaxy and crossing the nucleus. The optical extinction, measured from the Balmer decrement of the narrow  $H\alpha$  and  $H\beta$  components, is  $A_V = 4.2 \pm 0.4$  (Ward et al. 1980). Finally, evidence for coronal lines of [FeVII] and [FeX] have been found in the optical spectrum by Shuder (1980) and Winkler (1992).

The X-ray flux and spectrum were observed to vary during 16 years of observations performed with different satellites. As noted by Weaver et al. (1996; hereafter We96), since the time of HEAO-1 observations in 1978 (Mushotzky 1982), the 2–10 keV flux of NGC 2992 decreased by a factor of  $\sim 20$  until the ASCA observations in 1994, when it reached the lowest value. A similar decrease was also observed in the soft X-rays (We96). Before ASCA, the spectral shape exhibited some variations but on average it could be described as an absorbed ( $N_{\text{H}} \sim 10^{22} \text{ cm}^{-2}$ ) power law with photon index  $\Gamma \sim 1.7$  and an iron  $K\alpha$  line. The ASCA spectrum was however much different, with a very flat slope ( $\Gamma \sim 1.2$ ). These spectral variations have been interpreted by We96 as the evidence for radiation reprocessed by an optically and geometrically thick gaseous medium, e.g. the molecular torus invoked by unified models (Antonucci & Miller 1985). We96 measured a time lag between the Fe line and the continuum of  $10 \pm 4$  years, from which they estimate a distance of the torus from the central engine ( $\sim 3.2$  pc, that

however is still model-dependent). Flux variability in the infrared was found by Glass (1997), who in particular remarked a fading of the source from 1978 to 1996 apart from a strong outburst in 1988. All of this evidence suggests that before BeppoSAX observed NGC 2992 in 1997 and 1998, the AGN in the center was turning off.

In this paper we present an analysis of new BeppoSAX observations of NGC 2992 which show that the AGN is back to its previous high level of activity observed in 1978. The X-ray data are also complemented with optical and near-IR spectra obtained in a followup observation. The results of our analysis are compared with previous data in the literature.

We assume  $H_0 = 50 \text{ km s}^{-1} \text{ Mpc}^{-1}$  yielding a distance of 46 Mpc for NGC 2992.

## 2. X-ray data

### 2.1. New observations and data reduction

The four co-aligned Narrow Field Instruments (NFI) on board the Italian-Dutch satellite BeppoSAX (Boella et al. 1997a) span the broad X-ray energy range from 0.1 to 200 keV. The NFI include the Low Energy Concentrator Spectrometer (LECS; Parmar et al. 1997) and the Medium Energy Concentrator Spectrometer (MECS; Boella et al. 1997b), which both consist of a mirror unit plus a gas scintillation proportional counter and have imaging capabilities. The LECS instrument covers the energy range 0.1–10 keV with a spatial resolution of about  $\sim 1$  arcmin and a spectral resolution of 8% at 6 keV. The MECS instrument operates in the 1.8–10 keV band with the same spatial and spectral resolution of the LECS, but is two times more sensitive in the overlapping spectral range. The other NFI are a High Pressure Gas Proportional Counter (HPGSPC; Manzo et al. 1997) and a Phoswich Detector System (PDS; Frontera et al. 1997), which are direct-view detectors with rocking collimators. The HPGSPC (4–120 keV) has better energy resolution but is less sensitive than the PDS (13–200 keV). In this paper we will only take advantage of the LECS, MECS and PDS data. Errors, unless otherwise stated, will be given at the 90% confidence level for one interesting parameter ( $\Delta\chi^2 = 2.71$ ).

NGC 2992 was observed by BeppoSAX in 1997 (from December 1 to December 3) and in 1998 (from November 25 to November 27). The 1997 data and the 1998 data will be referred to as SAX1 and SAX2, respectively. For the SAX1 observation we will not take into account the LECS data due to poor statistics. Table 1 shows exposure times and net count rates (i.e. background subtracted) for both BeppoSAX observations. The MECS spectra for SAX1 and SAX2, and the LECS spectrum for SAX2 have been extracted with an aperture radius of 4 arcmin. The background subtraction files have been extracted with the same apertures from blank sky fields. The spectral data have been binned in order to have at least 20 counts per channel to validate the use of the  $\chi^2$  statistics.

**Table 1.** BeppoSAX observations of NGC 2992.

NFI <sup>a</sup>	Exposure time <sup>b</sup>	Net count rate <sup>c</sup>
<i>SAX1(1997)</i>		
MECS	72119	$0.082 \pm 0.001$
PDS	33820	$0.226 \pm 0.048$
<i>SAX2(1998)</i>		
LECS	22284	$0.411 \pm 0.004$
MECS	59245	$0.893 \pm 0.004$
PDS	27084	$1.405 \pm 0.005$

Errors on the counts are at  $1\sigma$  level.

<sup>a</sup>Narrow Field Instrument.

<sup>b</sup>In seconds.

<sup>c</sup>Background subtracted.

A possible source of contamination in the X-ray spectrum detected by BeppoSAX could be NGC 2993, which lies at about 2.9 arcmin from its companion NGC 2992. NGC 2993 has an optical magnitude comparable to that of NGC 2992 ( $\Delta m = 0.03$ ) and also shows optical narrow emission lines and radio emission (Ward et al. 1980). On the basis of the optical lines, NGC 2993 has been classified as a LINER (Durret 1990). Due to the uncertain nature of LINERs, which could host both thermal and non-thermal activity, NGC 2993 could contribute to the flux measured by BeppoSAX. However, since at 1415 MHz NGC 2993 is four times less luminous than NGC 2992 (Ward et al. 1980), and radio emission should not suffer from absorption, NGC 2993 should be intrinsically less luminous than NGC 2992 and its contribution to the observed X-ray spectrum should be small in every X-ray energy band from LECS to PDS. Also, the ROSAT PSPC data show that in the soft X-rays the flux of NGC 2993 is less than 5% of the NGC 2992 flux (We96), and an analysis of the ASCA SIS image of the NGC 2992 field has revealed that the emission of NGC 2993 is negligible also in the 2–10 keV band. Therefore, we consider the X-ray photons detected by BeppoSAX as entirely produced by NGC 2992.

### 2.2. Timing analysis

The flux of NGC 2992 was constant throughout the SAX1 observation in 1997 (Fig. 1). When a fit with a constant is performed to the SAX1 light curve, the result is  $\chi^2/dof = 9.4/14$  for a binning time of 10 ks. On the contrary the source exhibited short term variability in 1998 during the SAX2 observation, when it was in the high state: the source varied by a factor of  $\sim 1.4$  on timescales of  $7 \times 10^4$  s. A constant count rate is ruled out at  $> 99\%$  confidence level by the  $\chi^2$  test both for the LECS and MECS data.

The variability amplitude of NGC 2992 during the SAX2 observation was estimated by means of the normal-

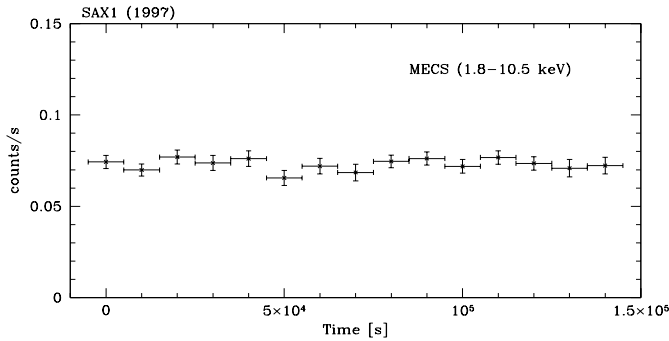


**Fig. 1.** Light curve for the MECS (1.8–10.5 keV) instrument during the SAX1 observation. The binning time is 10 ks; the light curve is not background subtracted.

ized “excess variance”  $\sigma_{rms}^2$  (see Nandra et al. 1997a for the definition of this quantity). In order to allow a comparison with the results of Nandra et al. (1997a) we have calculated  $\sigma_{rms}^2$  with a binning time of 128 s, which also ensures Gaussian statistics. For the 2–10 keV lightcurve  $\sigma_{rms}^2$  turned out to be  $9.7(\pm 0.3) \times 10^{-3}$ . This value is typical of Seyfert 1s with the same intrinsic 2–10 keV luminosity of NGC 2992 (Nandra et al. 1997a). We note that the value of  $\sigma_{rms}^2$  depends on the duration of the observation and that the exposures times for the Seyfert 1s sample of Nandra et al. (1997a) are all shorter than  $\sim 60$  ks, the MECS exposure time in SAX2. Therefore, in order to be consistent with the average exposure of the Nandra et al. (1997a) sample, we have considered different time intervals of  $\sim 30$  ks (first and second half of the observation and a central interval). We obtain a mean  $\sigma_{rms}^2$  of  $6.7(\pm 0.2) \times 10^{-3}$ , which still agrees with that observed in Seyfert 1s of comparable luminosity.

In order to check for spectral variations associated with the SAX2 short term variability, we have analyzed the ratio between the hard and soft X-ray photons (Hardness Ratio, HR) in different bands. When the HR is calculated comparing LECS to MECS data, one could not exclude some degree of spectral variability. However, HR variations are not detected when the HR is calculated only from MECS data. As an example (see Fig. 2), the HR between the MECS data in the 3.5–10.5 keV and 1.8–3.5 keV is constant at a high confidence level ( $\chi^2/dof = 6.1/11$ ). We note that the cross calibration between the LECS and MECS data is somewhat uncertain (see the next Section), and it might exhibit time variations. Therefore, we will consider the dispersion in the HR between the LECS and MECS data as an instrumental effect and extract only a time averaged spectrum.

### 2.3. Spectral analysis

#### SAX1 (1997)

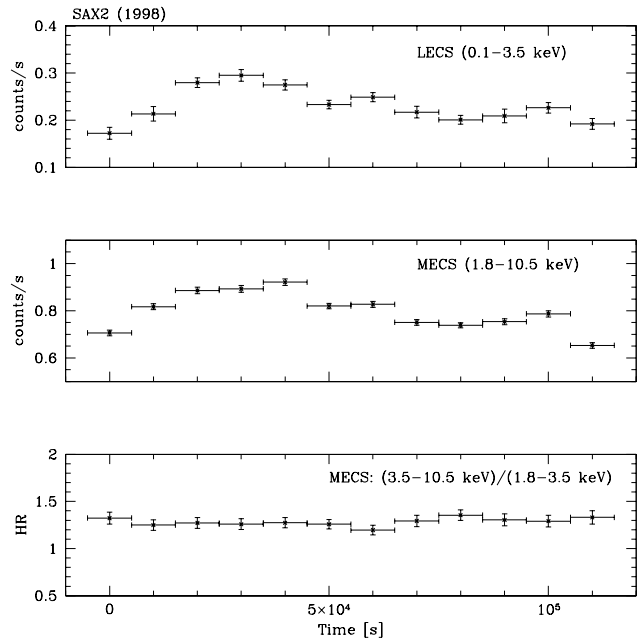


**Fig. 2.** Light curves for the LECS (0.1–3.5 keV) and MECS (1.8–10.5 keV) instruments and Hardness Ratio between MECS data during the SAX2 observation. The binning time is 10 ks; the light curves are not background subtracted.

The spectral analysis was performed by using the XSPEC 10.0 package. The MECS data in the 1.8–10.5 keV band and the PDS data in the 14–200 keV band were fitted simultaneously. A relative normalization factor was introduced between the PDS and MECS spectrum since the BeppoSAX instruments show some mismatches in the absolute flux calibration (the MECS is the best calibrated instrument). The energy ranges covered by the MECS and PDS do not overlap and so we cannot determine a cross calibration constant from the data. Instead, for the fitting procedure, we assumed a fiducial PDS to MECS normalization factor of 0.8 (released by the BeppoSAX Science Data Center). When fitting with an absorbed power law, strong residuals emerge at 6–7 keV suggesting a prominent iron line in the NGC 2992 spectrum. With the addition of a Gaussian iron line to the absorbed power law model we obtain a good fit to the data with  $\chi^2/dof = 149/144$ . The fit is shown in Fig. 3 and spectral parameters are quoted in Table 2 together with the hard X-ray flux and luminosity derived by the best fitting model. Spectral parameters are quoted in the rest frame.

The power law spectral index ( $\Gamma = 1.72 \pm 0.12$ ) is consistent with the typical value 1.7–1.9 for Seyfert galaxies (Nandra & Pounds 1994; Nandra et al. 1997b). The line broadening ( $\sigma_{K\alpha} = 0.18_{-0.14}^{+0.10}$  keV) is not highly significant (it is detected at  $\gtrsim 90\%$  confidence level,  $\Delta\chi^2 = 3.21$  with respect to a narrow fit with  $\sigma_{K\alpha} = 0$

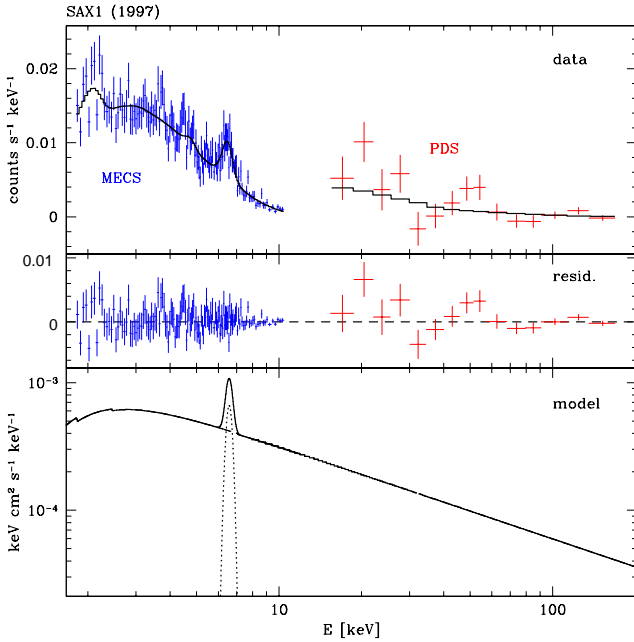


**Fig. 3.** Data and folded model (top), residuals (middle) and unfolded model (bottom) for the SAX1 observation.

keV). On the other hand, the energy of the Fe line,  $E_{K\alpha} = 6.62 \pm 0.07$  keV, is significantly higher ( $> 99.9\%$  confidence level,  $\Delta\chi^2 > 21$ ) than the value of 6.4 keV commonly observed in Seyfert galaxies (e.g. Nandra et al. 1997b; Turner et al. 1997) and expected from neutral or weakly ionized iron (below FeXVI). We note, however, that both the MECS2 and the MECS3 units (the MECS1 failed in May 1997) might be affected by an instrumental energy shift towards the blue of 0.05 and 0.08 keV at 6.6 keV respectively (SAX Cookbook: [http://www.sdc.asi.it/software/cookbook/cross\\_cal.html](http://www.sdc.asi.it/software/cookbook/cross_cal.html)). We have verified the significance of our results by calculating the confidence contours for the line energy versus the line width (shown in Fig. 4) and versus the photon index (not shown). Even applying a red shift of 0.05 or 0.08 keV to correct for the instrumental shift we find that  $E_{K\alpha} > 6.4$  keV at  $> 99\%$  confidence level. Therefore, evidence for iron emission from a highly ionized medium is provided by the data. The equivalent width of the line is very high,  $EW_{K\alpha} \sim 700$  eV and cannot be easily explained with current emission line models for a direct view of the nucleus (see Section 4).

We note that the PDS data are very noisy and do not allow to constraint significantly any reflection component in addition to the power law continuum.

#### SAX2 (1998)

The spectral data from the LECS, MECS and PDS were fitted simultaneously in the 0.1–3.5 keV, 1.8–10.5

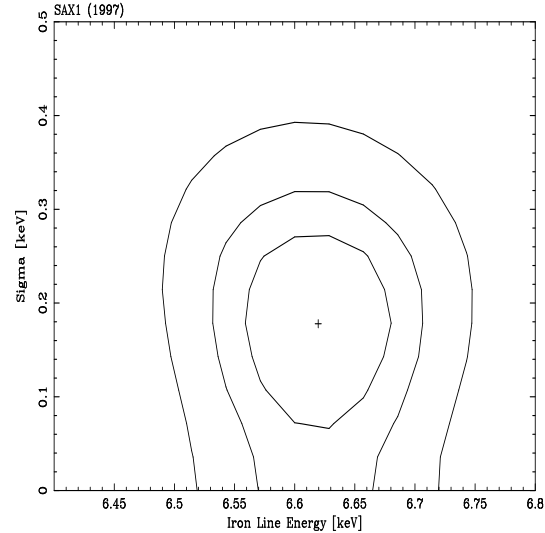


**Fig. 4.** Confidence contours of the iron line energy versus the line width for the SAX1 observation. The contour levels are 68%, 90% and 99% for two interesting parameters.

keV and 14–200 keV bands, respectively. As for the SAX1 observation, the PDS to MECS normalization was fixed to 0.8. The LECS to MECS normalization was determined by fitting simultaneously the LECS and MECS data in the overlapping band 1.8–3.5 keV; the obtained value was subsequently assumed for the spectral analysis. The procedure provides a model-independent LECS to MECS normalization of  $0.64 \pm 0.02$ . The typical values observed so far range from 0.65 (Malaguti et al. 1999) to 0.76 (Haardt et al. 1998; Guainazzi et al. 1999).

#### Fit with a power law and a Gaussian line

A simple absorbed power law model is unacceptable at  $> 97\%$  confidence level ( $\chi^2/dof = 431/374$ ) mostly because of the strong residuals at 6–7 keV due to the iron emission. The addition of a broad Gaussian iron line improves significantly the fit ( $\Delta\chi^2 \simeq 41$ ). The spectral parameters and fit are shown in Table 2 and Fig. 5, respectively. Some residuals at 15–20 keV could suggest that a reflection component is present. However, including a reflection continuum, obtained by means of the `pexrav` model in XSPEC (Magdziarz & Zdziarski 1995), is not strongly required by the data ( $\Delta\chi^2 \sim 1$  with the addition of one *dof*). The relative normalization  $R$  between the reflected and the direct continuum turns out to be low,  $R = 0.12$  ( $R \sim 1$  for a reflecting material covering  $2\pi$  of the source) and the steepening of the spectral index, which should be observed when adding a reflection continuum, is only  $\sim 1\%$ .<sup>1</sup>

<sup>1</sup> We verified that the relative normalization of the reflection component is low ( $R = 0.17$ ) also in the case of a ionized reflector, obtained by means of the `pexriv` model in XSPEC (Magdziarz & Zdziarski 1995).

**Table 2.** Spectral fits to the BeppoSAX data

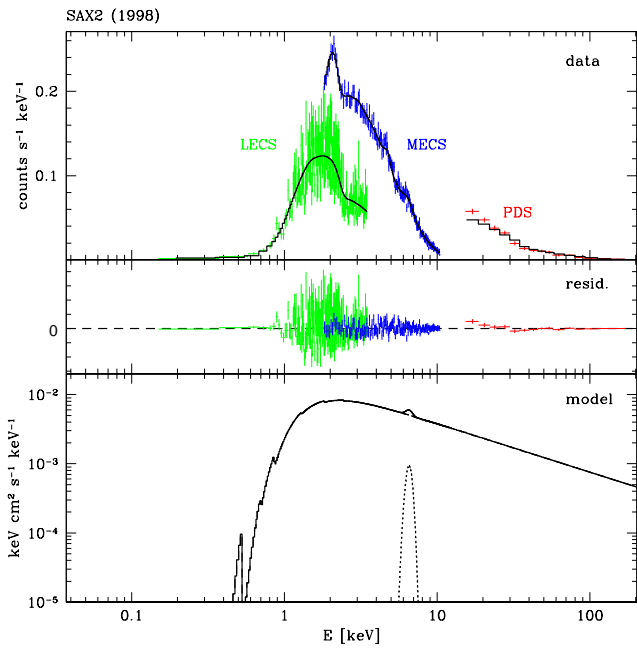
Model	$\Gamma$	$N_{\text{H}}$ [ $10^{22} \text{cm}^{-2}$ ]	$E_{\text{K}\alpha}$ [keV]	$\sigma_{\text{K}\alpha}$ [keV]	$EW_{\text{K}\alpha}$ [eV]	$f_{2-10 \text{ keV}}$ [ $10^{-11} \text{erg s}^{-1} \text{cm}^{-2}$ ]	$L_{2-10 \text{ keV}}$ [ $10^{42} \text{erg s}^{-1}$ ]	$\chi^2/dof$
<i>SAX1(1997)</i>								
apl+G1	$1.72^{+0.13}_{-0.12}$	$1.4^{+0.5}_{-0.4}$	$6.62^{+0.07}_{-0.07}$	$0.18^{+0.10}_{-0.14}$	$701^{+185}_{-163}$	0.63	1.8	149/144
<i>SAX2(1998)</i>								
apl+G1	$1.70 \pm 0.02$	$0.90 \pm 0.03$	$6.59^{+0.13}_{-0.15}$	$0.32^{+0.18}_{-0.06}$	$147 \pm 37$	7.4	20	390/371

apl+G1: absorbed power law plus Gaussian line. The luminosities are corrected for the absorption.

**Table 3.** The iron line complex in the BeppoSAX data.

Model	$E_{\text{K}\alpha}$ [keV]	$\sigma_{\text{K}\alpha}$ [keV]	$EW_{\text{K}\alpha}$ [eV]	$A_{\text{K}\alpha}$ [ $10^{-5} \text{ph s}^{-1} \text{cm}^{-2}$ ]	$\theta$ [deg]	$\chi^2/dof$
<i>SAX1(1997)</i>						
2 Gaussians	$6.4^f$	$0^f$	$120^{+100}_{-80}$	$1.4 \pm 1$		150/145
	$6.7^f$	$0^f$	$350^{+160}_{-130}$	$3 \pm 1$		
<i>SAX2(1998)</i>						
2 Gaussians	$6.4^f$	$0^f$	$80 \pm 30$	$6.5 \pm 2.3$		391/372
	$6.96^f$	$0^f$	$60 \pm 30$	$4.6 \pm 2.1$		
Fabian89	$6.4^f$		$208 \pm 56$	$16 \pm 5$	$46 \pm 7$	389/372
Laor91	$6.4^f$		$316 \pm 86$	$22 \pm 6$	$46 \pm 7$	390/372

<sup>f</sup>Frozen value. Fabian89: disc line model for a Schwarzschild black hole described by Fabian et al. (1989); Laor91: disc line model for a Kerr black hole described by Laor (1991).

**Fig. 5.** Data and folded model (top), residuals (middle) and unfolded model (bottom) for the SAX2 observation.

Similar to the SAX1 observation, the iron line peak is higher than 6.4 keV (although with a lower significance), while the line is definitely broad, ( $\sigma_{\text{K}\alpha} = 0.32^{+0.18}_{-0.06}$  keV) suggesting an emission from a relativistic accretion disc (Fabian et al. 1989). The confidence contours between the line energy and width for the SAX2 data are shown in

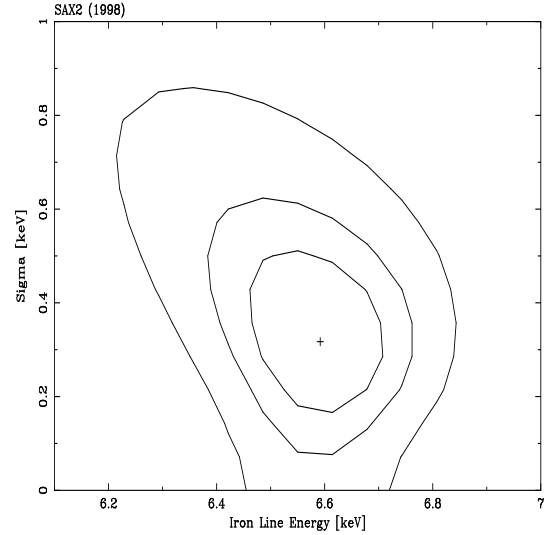
**Fig. 6.** Confidence contours of the iron line energy versus the line width for the SAX2 observation. The contour levels are 68%, 90% and 99% for two interesting parameters.

Fig. 6. The line equivalent width is  $EW_{\text{K}\alpha} = 147 \pm 37$  eV, which may be easily explained by accretion disc models where the matter is mildly ionized (Matt et al. 1992). The observed line energy peak above the value of 6.4 keV expected from neutral matter could be due to the Doppler shift in a relativistic disc inclined with respect to the line of sight.

*Disc line model*

Because of the above mentioned considerations, we performed fits with line profiles derived from relativistic disc models, under the assumptions of both a Schwarzschild and a Kerr metrics, i.e. non rotating and rotating black hole, respectively (see Tab. 3). Since the number of line parameters is relatively high and most of them would be poorly constrained in the fits, we fixed all the line parameters but the inclination angle  $\theta$  of the disc and the line normalization. The line was assumed to be cold ( $E_{K\alpha} = 6.4$  keV). In the Schwarzschild metric we assumed for the inner disc radius  $R_i = 6R_G$  (where  $R_G = GM/c^2$  is the gravitational radius and  $M$  is the black hole mass), which corresponds to the last stable orbit for an accretion disc around a Schwarzschild black hole. The outer disc radius was fixed to  $R_o = 1000R_G$  and the line emissivity was parameterized by  $R^{-q}$ , where  $R$  is the radius. The power law index  $q$  was assumed equal to 2.5, the mean value derived by Nandra et al. (1997b) for a sample of Seyfert 1 galaxies in the case of a Schwarzschild black hole. In the Kerr metric we assumed  $R_i = 1.23R_G$  (the last stable orbit in a rotating black hole metric),  $R_o = 400R_G$ , and  $q = 2.8$ , the average value derived from Nandra et al. (1997b) for a Kerr black hole. Fitting the iron line with relativistic disc models gives  $\chi^2/dof = 389/372$  for the Schwarzschild metric and  $\chi^2/dof = 390/372$  for the Kerr metric. Both models provide an adequate description of the data, comparable with the analytical broad Gaussian model. Remarkably, the inclination angle of the disc turns out to be the same both from the fits with the Schwarzschild and the Kerr metric:  $\theta = 46^\circ \pm 7$ . Therefore, the disc seems to be inclined and the energy of the line centroid can be explained by the relativistic Doppler shift of a cold line.

The estimate of disc inclination depends on the choice of inner radius and so we tested different values of  $R_i$  for the Schwarzschild and the Kerr metric. In both cases, the best fit is found when the inner radius correspond to the last stable orbit. The 90% upper limits on  $R_i$  are  $30R_G$  and  $5.3R_G$  for the Schwarzschild and the Kerr metric, respectively. If we calculate the values of  $\theta$  when  $R_i$  is fixed to its 90% upper limit, we find  $\theta = 65^{+25}_{-21}$  for the Schwarzschild metric and  $\theta = 44^{+4}_{-5}$  for the Kerr metric. Also, if the disc is ionized, the line centroid could be higher than 6.4 keV. Then, the Doppler boosting effect could be lower and the inclination estimate could be incorrect. We have therefore performed disc line fits fixing the line energy peak at 6.62 keV, i.e. the SAX1 line energy. The resulting values for  $\theta$  are  $36^{+7}_{-10}$  and  $38^{+6}_{-7}$  for a Schwarzschild and a Kerr black hole, respectively, fully consistent with  $46^\circ \pm 7$  derived previously for neutral disc models.

#### Line blend model

An alternate representation of the broad iron line feature could be a blend of lines emitted by iron at different

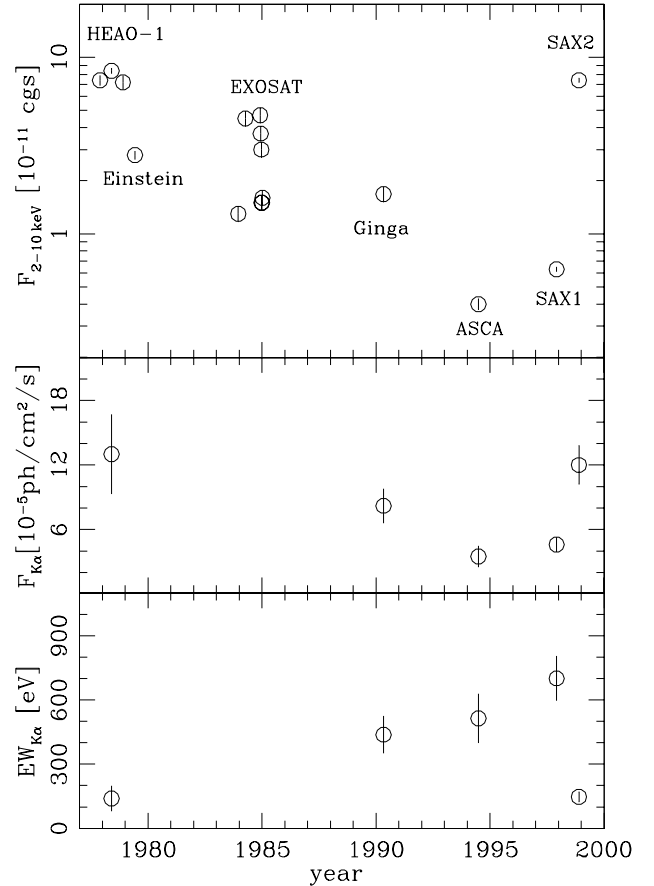


**Fig. 7.** From top to bottom, X-ray variability curve for the 2–10 keV continuum flux, the iron  $K\alpha$  line intensity, and the line equivalent width. The HEAO-1, Einstein, EXOSAT, Ginga and ASCA data are taken respectively from Mushotzky (1982), Turner et al. (1991), Turner & Pounds (1989), Nandra & Pounds (1994), Weaver et al. (1996). Errorbars are at the  $1\sigma$  level.

ionization stages. We performed a fit to the iron complex with two narrow Gaussians at 6.4 keV and 6.96 keV as expected from FeI–XVI and FeXXVI, respectively. This model provides an equally good fit to the data as for the broad Gaussian line fit ( $\chi^2/dof = 391/372$ ). Adding a 6.96 keV line describes the data better than having only the Fe  $K\beta$  component at 7.06 keV. The latter is not sufficient to explain the data at  $\sim 7$  keV. The addition of a third line at 6.68 keV expected from FeXXV is not significant.

#### 2.4. Comparison with previous results

Before the BeppoSAX observations, the X-ray flux of NGC 2992 decreased quite systematically from 1978 to 1994, when it was observed by ASCA. The flux measured

in SAX1 shows a modest increase with respect to the ASCA value, while a factor of  $\sim 12$  increase is detected between SAX1 and SAX2. The 2–10 keV flux measured by SAX2 is similar to that measured by HEAO-1 in 1978. The long term flux variability is shown in Fig. 7. The spectrum of NGC 2992 measured by SAX1 and SAX2 is an absorbed power law with  $\Gamma \sim 1.7$  and  $N_{\text{H}} = 10^{22} \text{ cm}^{-2}$  and is on average consistent with the results previously obtained by HEAO-1, Einstein, EXOSAT and Ginga, but not with the very flat ( $\Gamma \sim 1.2$ ) ASCA spectrum in 1994. The peculiar spectrum detected by ASCA has been interpreted by We96 as evidence for a strong reflection continuum superposed to a weak power law continuum with  $\Gamma \sim 1.7$ . The reflection continuum should represent the echo of the past brightness of the source. No significant evidence for short term variability was observed in the ASCA data (We96).

An example of a similar flux and spectral variation has been observed in NGC 4051 (Guainazzi et al. 1998), where a drop out of a factor of  $\sim 20$  in the 2–10 keV flux was accompanied by a spectral change from a power law with  $\Gamma \sim 1.9$  to a pure reflection continuum.

The iron line in the BeppoSAX spectrum is significantly different from that detected by ASCA. We96 found that the line in the ASCA spectrum is cold ( $E_{\text{K}\alpha} = 6.42 \pm 0.04 \text{ keV}$ ), narrow ( $\sigma_{\text{K}\alpha} < 0.06 \text{ keV}$ ) and has an equivalent width of  $EW_{\text{K}\alpha} = 514 \pm 190 \text{ eV}$ . Because of the line narrowness and its high equivalent width, We96 argued in favor of iron emission from a distant torus, that must be characterized by a large column density to produce the observed iron line and the cold reflection that flattens the ASCA spectrum. The line energy observed by Ginga in 1990 (Nandra & Pounds 1994) is  $6.43 \pm 0.16 \text{ keV}$ , consistent with neutral iron emission. Because of the poor energy resolution of the Ginga LAC the line width was not determined. No useful information about the line energy and width can be extracted by HEAO-1 data (Weaver, Arnaud & Mushotzky 1995). A summary of the variations of the iron line parameters along all the X-ray observations of NGC 2992 is shown in Fig. 7.

### 3. Optical and near-IR data

As soon as we received the last set of BeppoSAX data and realized the enhanced X-ray activity with respect to the previous BeppoSAX observation, we submitted a target of opportunity proposal to the European Southern Observatory to observe the behavior of various nuclear components such as the broad line region and the hot dust emission. As discussed in this Section the observation was performed in early January 1999, i.e. about 1.5 months after the BeppoSAX observation.

#### 3.1. New observations and data reduction

Near Infrared and optical observations of NGC 2992 were performed at the ESO New Technology Telescope (NTT).

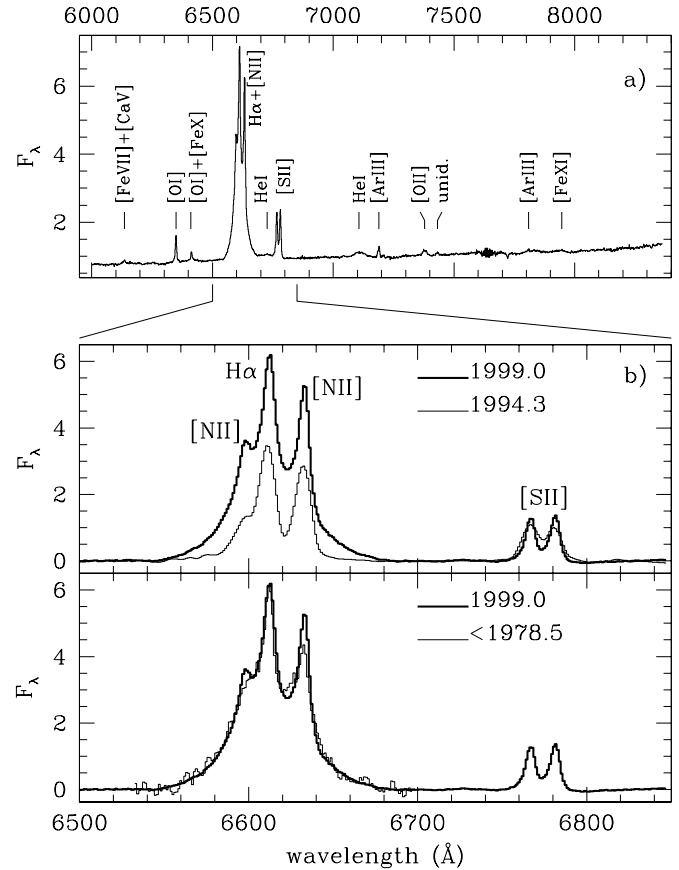


**Fig. 8.** Top, optical spectrum of NGC 2992 obtained by us in January 1999. Middle, comparison of our spectrum with that obtained by Allen et al. (1999) in 1994, i.e. at the time of the minimum X-ray activity. Bottom, comparison of our spectrum with that obtained by Veron et al. (1980) prior to 1978, i.e. when the nucleus was in the former high X-ray state.

The infrared data were collected on January 7, 1999 with photometric conditions using the imaging and spectroscopic modes of SOFI, equipped with a Hawaii HgCdTe 1024x1024 detector.

Images in the J, H and Ks filters were obtained with the small field objective yielding a  $0''.144/\text{pix}$  scale. The seeing during the observations was  $\sim 0''.7$ . Observations consisted of several on-source exposures interleaved with sky exposures while stepping the object on the detector by  $\sim 20''$ . The total on-source integration time was of 200 s in J and 120 s in H and Ks. Flat-field correction was performed using differential dome exposures and the sky was subtracted from each on-source frame. Images were then co-aligned by using stars present in the field of view and coadded. Flux calibration was performed using the standard star SJ9138 (Persson et al. 1998).

Spectral observations were performed with the Red and Blue grism yielding a dispersion of  $10 \text{ \AA}/\text{pix}$  in the  $1.52\text{--}2.52 \text{ }\mu\text{m}$  range and  $7 \text{ \AA}/\text{pix}$  in the  $0.95\text{--}1.64 \text{ }\mu\text{m}$  range. The pixels subtended  $0''.276$  along the  $1''$  slit and

the resolving power was  $\sim 600$  at  $2.2 \mu\text{m}$  and  $\sim 500$  at  $1.25 \mu\text{m}$ . Observations consisted of several couples of exposures in which the object was moved at two different positions along the slit, in order to perform sky subtraction. On-chip integration time was 120 s resulting in a total, on-source integration time of 960 s. Data were flat fielded with spectroscopic dome exposures and sky subtracted. Correction for optical distortion of the slit direction and wavelength calibration were performed with Xenon and Neon arc exposures. The zero point of the wavelength calibration was then checked using the OH sky lines (Oliva & Origlia 1992). Residual sky emission was removed by fitting a linear polynomial along the slit. Correction for instrumental response and telluric absorption, and flux calibration were performed by using the G1V star HR3916. The intrinsic stellar features were then canceled by dividing for the sun spectrum according to the prescription described by Maiolino, Rieke & Rieke (1995). The FWHM ( $1''$ ) of the point spread function along the slit was estimated by using the wings of the broad lines which are emitted from a spatially unresolved region. The final spectrum was then extracted in a  $1'' \times 2''$  aperture centered on the nucleus which corresponds to the slit width by  $2 \times \text{FWHM}$ .

The optical spectra were collected on January 12, 1999 with photometric conditions using EMMI in the Low Resolution Spectroscopy (RLD) mode with grating #6. The projected pixel size of the Tektronic 2048x2048 CCD was  $0''.27$  along the slit and  $1.2 \text{ \AA}/\text{pix}$  along dispersion. The slit width was  $2''$  yielding a resolution of  $R \sim 700$  at  $6500 \text{ \AA}$ . The slit was centered on the galaxy nucleus with a position angle of  $120 \text{ deg}$ . The  $6000\text{-}8400 \text{ \AA}$  spectrum was obtained by merging two different exposures of 1200 s in order to remove cosmic rays. Data reduction was performed using standard procedures for CCD long-slit spectra, i.e. bias subtraction, flat field correction, rectification of the slit direction and wavelength calibration. Correction for instrumental response and flux calibration were performed using the spectrophotometric standard star LTT3864 (Hamuy et al. 1992, 1994). The final spectrum of the nuclear region was extracted, with the same procedure adopted for the IR spectra, in a  $2'' \times 1''.4$  aperture.

### 3.2. Broad lines analysis

Fig. 8a shows the optical spectrum of NGC 2992 obtained with EMMI. Fig. 8b shows the continuum subtracted zoom of the spectrum around  $\text{H}\alpha$ , that clearly shows the presence of a prominent broad component of  $\text{H}\alpha$ . For comparison Fig. 8b also shows the nuclear spectrum obtained by Allen et al. (1999) in March 1994, i.e. at the minimum activity ever observed in the X-rays. The latter spectrum was scaled to match the intensity of the  $[\text{SII}]$  doublet in our spectrum. Although Allen's spectra have slightly lower spectral resolution ( $\sim 550$ ) their spectrum clearly shows a much weaker, if any, broad component of  $\text{H}\alpha$ . In contrast,

our spectrum is remarkably similar to the spectrum obtained by Veron et al. (1980) prior to 1979<sup>2</sup>, i.e. probably when the nucleus was at the same level of X-ray activity as in late 1998 (Sect. 2). We deblended the broad and narrow components of  $\text{H}\alpha$  by using a multiple Gaussian fit. The narrow components are unresolved at our spectral resolution. Some relevant results of the fit are reported in Tab. 4 (additional information is given in the Appendix) and are compared with the values obtained by Veron et al. (1980) in the former high activity phase. The ratio between broad and narrow  $\text{H}\alpha$  are nearly identical for the two observations. Also Allen et al. spectrum seems to require a broad  $\text{H}\alpha$  component of about the same width as that found in our spectrum, but about 10 times weaker.

The optical spectrum also shows a variety of other lines that are marked in Fig. 8a. The analysis of flux variation of some coronal lines (such as  $[\text{FeVII}]\lambda 6087 \text{ \AA}$ ,  $[\text{FeX}]\lambda 6374 \text{ \AA}$ ,  $[\text{FeXI}]\lambda 7892 \text{ \AA}$  and  $[\text{SiVI}]\lambda 1.96 \mu\text{m}$ ) with respect to the past would provide interesting constraints on the size of the Coronal Line Region, that is expected to be intermediate between the BLR and the NLR. Unfortunately, the quality of previous spectra is too poor to provide useful constraints to the flux of such coronal lines. However, in the Appendix we provide the fluxes of all the lines that are detected and identified in our spectrum and that could be useful for comparison with future monitoring.

Fig. 9 shows the infrared spectrum taken with SOFI at ESO, where we combined the blue and red spectra. The spectrum shows a wealth of features, most of which are observed for the first time in this galaxy thanks to the much improved sensitivity of this observation with respect to previous data. In this paper we only discuss those features that are relevant to the issue of the burst observed in the X-rays. However, in the Appendix we report the list of the lines, along with their fluxes, that we detected and identified in the spectrum.  $\text{Pa}\beta$  is the most suitable line for studying the profile of near-IR hydrogen lines, since it is relatively strong, isolated, and in a good atmospheric window. We fitted the  $\text{Pa}\beta$  with two Gaussians (broad and narrow, unresolved) whose parameters were frozen to the same values obtained for  $\text{H}\alpha$  except for their normalization. As reported in Tab. 4 the observed  $\text{Pa}\beta$  can be almost fully accounted for by the broad component alone, while the narrow component contributes for only  $\sim 7\%$ , much lower than in the case of  $\text{H}\alpha$ . In Tab. 4 we also compare our result with those obtained by Rix et al. (1990) in 1989, when the nucleus was mildly active, and with the result of Goodrich et al. (1994) in May 1992, i.e. when the nucleus was close to its minimum activity. Although this comparison should be considered with caution because of different instrumental setup and lower sensitivity of past observations, there is an apparent correlation between the

<sup>2</sup> The date of the observation is not given in the Veron et al. paper.

**Table 4.** Properties of the optical and near infrared hydrogen lines.

	2190	(1999.0) <sup>b</sup>
FWHM[ $H\alpha(broad)$ ] <sup>a</sup>	2620	(1994. - near minimum) <sup>c</sup>
	2030	(<1978.5 - former active phase) <sup>d</sup>
	6.8	(1999.0) <sup>b</sup>
$\frac{H\alpha(broad)}{H\alpha(narrow)}$	0.7	(1994. - near minimum) <sup>c</sup>
	6.0	(<1978.5 - former active phase) <sup>d</sup>
	17.2	(1999.0) <sup>b</sup>
$\frac{Pa\beta(broad)}{Pa\beta(narrow)}$	1.7	(1992.4 - near minimum) <sup>e</sup>
	3.3	(1989. - intermediate phase) <sup>f</sup>
$\frac{Br\gamma}{Pa\beta}$	0.22	(1999.0) <sup>b</sup>
$\frac{Pa\beta(broad)}{H\alpha(broad)}$	0.30	(1999.0) <sup>b</sup>

<sup>a</sup> Full width half maximum in km/s.<sup>b</sup> This work.<sup>c</sup> Allen et al. (1999).<sup>d</sup> Veron et al. (1980).<sup>e</sup> Goodrich et al. (1994).<sup>f</sup> Rix et al. (1990).**Table 5.** Near infrared photometry of the nucleus.

Epoch	Aperture	J	H	K	J-K	H-K
1999.0 <sup>a</sup>	2''	12.52	11.50	10.63	1.89	0.87
1990.0 <sup>a</sup>	12''	10.94	10.01	9.45	1.49	0.56
1988.3 (burst) <sup>b</sup>	12''	11.00	9.93	9.21	1.79	0.72
1987.6 (quiesc.) <sup>b</sup>	12''	11.18	10.21	9.77	1.41	0.44

<sup>a</sup> This work.<sup>b</sup> Glass (1997)

$Pa\beta(broad)/Pa\beta(narrow)$  ratio and the level of nuclear activity as traced by the hard X-rays.

### 3.3. The hot dust emission

The most interesting feature of the near infrared images (not shown) is a powerful nuclear emission characterized by very red colors. More specifically, within the central 2 arcseconds we measure  $H-K = 0.9$  and  $J-K = 1.9$ , while typical galaxy colors are  $H-K = 0.2$  and  $J-K \simeq 0.6$ . Nuclear dust absorption is probably partly responsible for such red colors, but very likely hot dust emission in the H and K bands also contributes significantly (see Oliva et al. 1995, Maiolino et al. 1998, Thatte et al. 1997 for similar cases in other objects). This interpretation is supported, in the specific case of our observations, by the near-IR spectrum: the stellar CO absorption bands above  $2.29 \mu\text{m}$  and in the H band (e.g. at  $1.62 \mu\text{m}$ ) are much weaker than generally observed in normal galaxies. In particular, the equivalent width of the  $^{12}\text{CO}(2-0)$  band is only  $7.5 \text{ \AA}$ , while in normal galaxies this quantity generally ranges between 12 and  $14 \text{ \AA}$ . This effect has been observed in other AGNs and is generally ascribed to hot dust emission

diluting the stellar features in the near-IR (Oliva et al. 1995, Oliva et al. 1999).

The burst observed by Glass (1997) in 1988 during his near-IR monitoring also had features typical of hot dust emission, indeed the burst had much higher power in the K and L bands than in H and J. In Tab. 5 we compare the magnitudes observed by us with the magnitudes measured by Glass at the maximum, in the same aperture, during the 1988 burst, and the background galaxy magnitudes that corresponds to the minimum values observed during the near-IR monitoring.<sup>3</sup> The magnitudes measured by us are intermediate between the maximum and the minimum value observed. The physical implications are discussed in the next Section.

## 4. Discussion

### 4.1. Long and short term variability in the X-rays

The data collected by BeppoSAX suggest that an AGN has revived in the center of NGC 2992. The 2–10 keV flux

<sup>3</sup> With regard to the K band magnitudes, note that we used a filter (K-short) slightly different from that used by Glass, that is less sensitive to the hot dust emission at long wavelengths.

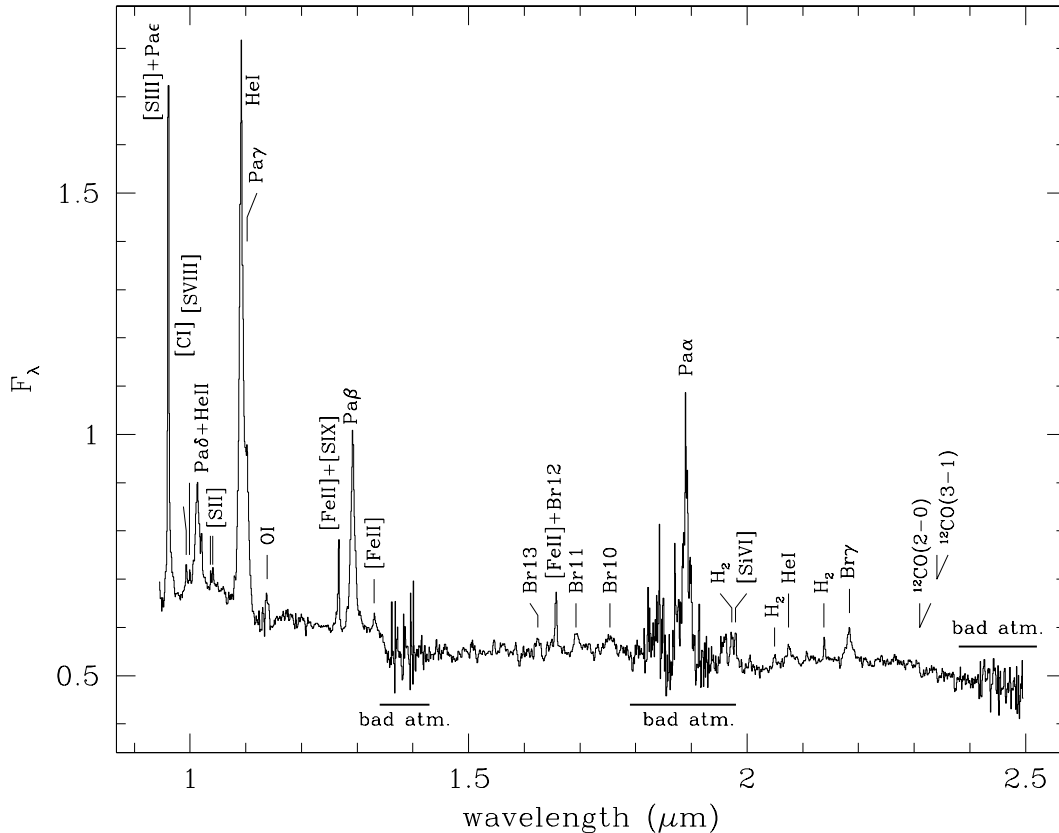


**Fig. 9.** Near infrared spectrum of NGC 2992 obtained in January 1999.

of the source systematically decreased by a factor of 19–20 between 1978 and 1994 and then increased by the same amount from 1994 to 1998. During the same time intervals the iron line flux changed by a factor  $\sim 3.5$ . Therefore, in 1998 both the continuum and the iron  $K\alpha$  line intensity have settled back to the same values observed in 1978. This coincidence of fluxes could indicate that in the high state the luminosity of NGC 2992 is close to the maximum luminosity achievable, i.e. its Eddington limit. However further observations would be needed to confirm this hypothesis.

The rebuilding of the AGN is also supported by the analysis of the short term variability of NGC 2992. In 1998, during the high state SAX2 observation, the source exhibited significant flux variations with an amplitude typical of Seyfert 1s (Nandra et al. 1997a), while in the low states observed in 1994 and 1997 no evidence for short term variability was found. The SAX2 variability is consistent with a scenario where we are observing the AGN directly through an absorbing medium. This situation is frequently observed in other objects with an intermediate Seyfert type classification in the optical and a column density of  $N_{\text{H}} \sim 10^{22} \text{ cm}^{-2}$  in the X-rays (e.g. NGC 526A, NGC 7314 and MCG -5-23-16; Turner et al. 1997).

The lack of variability throughout the SAX1 observation could suggest that during the rebuilding phase of the AGN the geometry of the central region and the ac-

cretion processes were different from those observed in SAX2. Ptak et al. (1998) found that Low Luminosity AGNs (LLAGNs) do not follow the Nandra et al. (1997a) relation, i.e. LLAGNs do not show time variability. These authors ascribed the behaviour of LLAGNs to the presence of an Advection Dominated Accretion Flow (ADAF; see Narayan, Mahadevan & Quataert 1998 for a review) in their nuclei. We note, however, that the X-ray luminosity of NGC 2992 during the SAX1 observation ( $1.8 \times 10^{42} \text{ erg s}^{-1}$ ) is rather high compared with the typical luminosity of LLAGNs ( $10^{40} - 10^{41} \text{ erg s}^{-1}$ ). Furthermore, the ADAF scenario would hardly explain the prominent iron line detected in SAX1. Therefore, we favor the interpretation that ascribes the lack of variability in SAX1 to a distant and extended forming disc (and, possibly, an extended corona) rather than to an ADAF. Another possibility is that during the SAX1 observation the nucleus was in a transition state where both a central ADAF and a distant accretion disc were present.

Since the long term variations amplitude of the iron line flux is different from that of the continuum, it is very likely that an accretion disc is not the only source of the line photons. Indeed, the disc is close to the X-ray primary source and it should reprocess the primary radiation on very short timescales of minutes or hours. Thus, one should expect long term variations of the disc line flux identical to those of the continuum. An iron emission

from a distant medium, such as the obscuring torus postulated by the unified model, which lags the direct flux by timescales of years is therefore very plausible. We96 derived that the torus must have a geometry and distance from the nuclear source such that it produces a time lag of  $\sim 10$  yr in the variation of the Fe line with respect to the continuum. Although this is likely to be the case for the narrow line detected by ASCA, no constraints are present on the line width detected by HEAO-1 in 1978. We note that if a disc component is present in the HEAO-1 data, the estimate of We96 is likely to be a lower limit on the torus distance.

#### 4.2. Iron line and reflection continuum diagnostics in SAX1

The SAX1 observation could have caught NGC 2992 during the rebuilding phase of the AGN. The spectral continuum is similar to that of normal AGNs, while the iron feature is peculiar and cannot be easily explained in the framework of iron emission from an accretion disc or a molecular torus (Ghisellini, Haardt & Matt 1994). Indeed, the line is narrow in contrast with standard disc models. Furthermore, the line energy ( $E_{K\alpha} = 6.62 \pm 0.07$  keV) is not consistent with 6.4 keV as expected from the neutral iron in the torus.

Such a narrow and warm line could be produced by ionized iron in a warm scattering material via resonant scattering (Matt, Brandt & Fabian 1996). A problem with this model is related to the observed line equivalent width of  $\sim 700$  eV. The equivalent width of the resonant lines predicted by Matt et al. (1996) can be as high as a few keV if the nuclear source is obscured and only the scattered continuum observed. This is the case of NGC 1068 (Ueno et al. 1994; Matt et al. 1997) which is a Compton thick AGN. However, when the nuclear source is directly viewed, as in the case of NGC 2992, the equivalent width of the resonant lines is predicted to be at most  $\sim 100$  eV (Krolik & Kallman 1987).

Another possible explanation of the line properties in SAX1 is to assume a blending between a narrow cold component from the molecular torus and a narrow hot component from a distant ionized disc which is forming. The narrowness of the line can be explained by assuming that the accreting material which is going to rebuild the disc is still far from the central black hole and so the line does not suffer from strong Doppler or gravitational broadening. We have therefore fitted the SAX1 line data with two narrow Gaussians at 6.4 keV and 6.7 keV, also adding a reflection continuum. In order to compare the intensity of the 6.4 keV line and of the reflection continuum with the ASCA values, we have fixed the spectral index to  $\Gamma = 1.7$ , as adopted by We96 for the ASCA data. We obtain a fit as good as the single Gaussian line fit; the equivalent widths and intensities of the two lines are respectively:  $A_{6.4\text{keV}} = 1.4(\pm 1) \times 10^{-5}$  photons  $\text{cm}^{-2} \text{s}^{-1}$ ,

$EW_{6.4\text{keV}} = 120_{-90}^{+100}$  eV,  $A_{6.7\text{keV}} = 3(\pm 1) \times 10^{-5}$  photons  $\text{cm}^{-2} \text{s}^{-1}$ ,  $EW_{6.7\text{keV}} = 350_{-130}^{+160}$  eV. The 6.4 keV line intensity is lower than the ASCA value, qualitatively in agreement with the idea that this is a fading reprocessed component (quantitatively, the fading of the Fe cold line depends on the detailed geometry of the torus). The comparison between the ASCA and SAX1 reflection continua is less straightforward since a disc contribution is expected in SAX1 in addition to the torus one. However, we note that in SAX1 data there is scope for including a torus reflection normalization lower than the ASCA value.

Both the centroid energy and equivalent width of the 6.7 keV component could be explained by means of ionized disc models (Matt, Fabian & Ross 1993). The ionization structure of the disc is basically determined by the ionization parameter  $\xi$  defined as following:

$$\xi = 4\pi F_{\text{h}}/n_{\text{H}}, \quad (1)$$

where  $n_{\text{H}}$  is the hydrogen number density of the disc and  $F_{\text{h}}$  is the hard X-ray flux impinging on the disc surface. When  $\xi$  is of the order of  $\sim$  a few hundreds (in units of  $\text{erg cm s}^{-1}$ ), the iron ionization state is mostly below FeXVI: the line energy is at  $\sim 6.4$  keV and the equivalent width is  $\sim 150$  eV as expected for cold discs. For  $\xi \sim 2000$  the emission is dominated by FeXXV: the line energy is close to 6.7 keV and the equivalent width is as high as 350–400 eV since most of the elements lighter than iron are fully stripped and do not absorb the iron line photons. Finally, when  $\xi \sim 5000 - 10000$  the bulk of the line is emitted by FeXXVI: the line energy is at 6.96 keV and the equivalent width has decreased to  $\sim 100$  eV, since a large fraction of iron is now completely bare. Therefore, the 6.7 keV line in the SAX1 spectrum is consistent with emission from a ionized disc with  $\xi \sim 2000$ . Following Matt et al. (1992), if we assume that the hard X-ray source (possibly an extended corona of relativistic electrons, Haardt & Maraschi 1991) is located at  $\sim 50R_{\text{G}}$  above the disc plane, we can estimate a hydrogen density of  $n_{\text{H}} \sim 10^{14} \text{ cm}^{-3}$  for these stages of the rebuilding disc.

#### 4.3. Iron line and reflection continuum diagnostics in SAX2

The SAX2 spectrum of the high state is consistent with the typical X-ray spectrum of AGNs, suggesting that the rebuilding of the AGN phenomenon is almost completed. The iron line profile in SAX2 is consistent with that expected from cold accretion disc models. The hard X-ray luminosity has increased by an order of magnitude with respect to the SAX1 data, and  $\xi$  is expected to be of the order of  $\sim 200$  as for cold discs. Therefore, the full-developed accretion disc in SAX2 should be about two order of magnitude denser than the forming disc observed in SAX1. If we assume that at the time of the ASCA observation the AGN was in a completely quiescent phase, we can consider

the time interval between the ASCA and SAX2 observations as an upper limit to the timescale for the rebuilding of the disc. Also, the time interval between SAX1 and SAX2 provide a lower limit to the rebuilding timescale. As a result, the rebuilding timescale turns out to range from 1 to 5 years. Since the obscuring torus should reside at a distance of  $\sim 3.2$  pc (i.e. 10 ly) from the central source (We96), in SAX2 (1998) any narrow iron line from the torus, in addition to the disc line, is expected to be weaker than that detected by We96 in 1994. We have verified this to be the case. Also, the reflection component produced by the torus is now completely diluted by the nuclear and disc continua. The best fit inclination angle for the disc, as estimated from the iron line profile, is  $\theta = 46^\circ \pm 7$ . Provided that the accretion disc and the molecular torus are coplanar, the inclination angle measured from the disc line profile is in agreement with the unified schemes where intermediate Seyfert types could be active nuclei observed through the rim of the torus. The moderate X-ray absorption of  $N_{\text{H}} \sim 10^{22} \text{ cm}^{-2}$  could be indeed produced by the outer boundary of an optically thick torus. Alternately, the X-ray absorption could be produced by the gas associated to the dust lane observed in the host galaxy and crossing the nucleus. In line with this interpretation is the fact that the optical extinction inferred from the optical and infrared *narrow* lines is close to that expected from the gaseous column density derived from the X-rays (for a Galactic gas-to-dust ratio). The fact that the extinction measured toward the BLR is similar to the extinction affecting the NLR is also in favor of this interpretation. The nature of the absorber will be discussed more in detail in the next section.

We note that NGC 2992 could be one of the first sources where there is evidence for two distinct absorbers in different spatial regions: the first (along our line of sight) is associated to the interstellar gas extended on the 100 pc scale, and the second (out of the line of sight) is associated to the thick molecular torus on parsec scales. This phenomenology has been recently observed also in the Seyfert 1.8 galaxy NGC 1365 (Risaliti, Maiolino & Bassani 1999).

In SAX2 one problem related to the AGN scenario with an accretion disc model is that the reflection continuum produced by the disc and associated to the iron line is weaker than expected. The relative normalization between the direct and reflected continuum is  $R = 0.12$ , which is in contrast with the value of 1 predicted by an isotropic source illuminating a plane-parallel semi-infinite slab and suggested by the line equivalent width. If we introduce a high-energy spectral cut off to  $E_c = 150$  keV, the minimum e-folding energy value to maintain a statistically good fit, then  $R$  increases only to 0.4, which is still a low value. Two possibilities to solve this problem are to introduce an iron overabundance or to assume that we are observing the source through a dual absorber with column densities of  $\sim 10^{22-23} \text{ cm}^{-2}$ . The combination of a dual absorber, a canonical power law with  $\Gamma \sim 1.9$ , and

a reflection component could indeed mimic a flatter power law with  $\Gamma \sim 1.7$ . In this scenario the line photons could be produced both in reflection by the accretion disc and in transmission by the dual absorber. Examples of complex absorbers are found in the X-ray spectrum of NGC 2110 (Malaguti et al. 1999) and NGC 5252 (Cappi et al. 1996).

In Section 2 we showed that another representation of the iron line complex of SAX2 could be a blending between lines emitted by different iron ions. In particular, two narrow lines at 6.4 keV and at 6.96 keV, deriving from the low and highly ionized iron respectively, adequately fit the data. However, this scenario seem to be disfavoured since the intensity of the cold line at 6.4 keV is higher than expected. Indeed, the narrow cold line at 6.4 keV in SAX2 should be the signature of the emission from the torus and, therefore, should be weaker than that measured by ASCA, just because the nuclear continuum had been falling until 1994 and there is a 10 years time lag between narrow-cold Fe line and continuum (We96). Actually, the 90% lower limit to the intensity of the narrow cold line measured in SAX2 (see Table 3) is higher than the 90% upper limit to the ASCA line intensity ( $3.5 \times 10^{-5} \text{ photons cm}^{-2} \text{ s}^{-1}$ ) derived by Turner et al. (1997).

#### 4.4. The BLR and the hot dust emission

Unfortunately, the optical and near-infrared follow up performed by us cannot provide tight constraints to the size of the Broad Line Region and of the hot dust emitting region because we do not know exactly the time of the X-ray burst; we only know that the transition occurred between December 1997 and November 1998. Nonetheless our data provide some interesting information on the geometry of the circumnuclear region.

Reverberation studies have shown that the BLR has typical sizes  $R_{\text{BLR}} = 0.02 L_{45}^{1/2} \text{ pc}$  (Netzer 1990). NGC 2992 has a hard X-ray luminosity of  $L_{2-10\text{keV}} = 2 \times 10^{43} \text{ erg s}^{-1}$ , that translates into a bolometric luminosity of about  $L_{\text{bol}} = 2 \times 10^{44} \text{ erg s}^{-1}$  (Mulchaey et al. 1994). Therefore the expected size of the BLR is about 0.01 pc. Our detection of broad lines both in the optical and in the near-IR spectra can only provide an upper limit to the size of the BLR, given by the fact that the burst cannot be older than about 1 yr at the time of the optical-IR observations and, therefore,  $R_{\text{BLR}}(\text{NGC 2992}) < 0.3 \text{ pc}$  that is fully consistent with the expected value of 0.01 pc derived above. However, we note that reverberation studies are generally more sensitive to the inner region of the BLR, since this is the region where rapid line variations are better detected. Fig. 8 and Tab. 4 show that the broad lines detected by us are at the same level as those observed by Veron et al. (1980) during the former high level state prior to 1978. This implies that the whole BLR has already been fully ionized and, therefore, the upper limit of 0.3 pc does not simply apply to the average BLR radius or to the “cross-correlation” size (that is usually the quantity

measured by reverberation mapping), but this upper limit applies also to the outer radius of the BLR.

As discussed in the former Section both the IR spectrum and images clearly show evidence for hot dust emission. Although dust close to the sublimation limit ( $T \sim 1500$  K) has the highest emissivity at  $\sim 2 \mu\text{m}$ , the increasing volume of emitting dust at lower temperatures implies that a large contribution to the K band emission comes also from regions at lower temperatures (down to 400 K), hence at larger distances. The K and H band fluxes observed by us are not at the maximum level observed by Glass (1997) during the 1988 burst<sup>4</sup>, implying that in January 1999 the hot dust emission is still in the raising phase. The region of dust close to the sublimation limit ( $T > 1000$  K) was already heated. Instead, the regions with dust at temperatures around 500 K, that significantly contribute to the K band emission, were not active yet. According to the dust equilibrium temperature obtained by Laor & Draine (1993), dust at temperatures around 500 K should be located at a radius of about  $R_{\text{pc}} \simeq 0.36 L_{46}^{1/2} T_{1500}^{-2.5} = 0.8$  pc, given the luminosity of NGC 2992, and therefore it is not surprising that we do not see the whole K band emission yet, considered that the burst was not older than 1 year at the time of the infrared observations. The dust close to the sublimation limit ( $T \simeq 1500$  K) is expected to be located at a distance of  $\sim 0.05$  pc, fully consistent with the upper limit of 0.3 pc that we can infer from the maximum time delay between the X-ray burst and the infrared observation.

Generally, the sizes of BLR and hot dust region have been estimated independently for different objects. However, Netzer & Laor (1993) proposed that the relative dimensions of these two regions are related and, more specifically, that the outer boundary of the BLR is located just inside the sublimation radius of the dust grains. This model was proposed to explain the apparent gap between the BLR and the NLR with almost no line emission. Our optical and infrared followup supports this model. Indeed, as discussed above, the BLR appears to be fully formed when the hot dust region is still forming, consistent with the fact that the BLR outer radius is smaller than the hot dust emitting region.

#### 4.5. Optical extinction

Finally, we can use the ratio between the broad lines to estimate the absorption toward the BLR and compare it with the absorbing column density derived from our X-ray observations. As discussed in the previous Section and as shown in Tab. 4, in the near IR the hydrogen lines are completely dominated by the broad components. By as-

suming an intrinsic ratio 0.16 between  $\text{Br}\gamma$  and  $\text{Pa}\beta$ , and the extinction curve in Rieke & Lebofsky (1985), we infer  $A_V(\text{BLR}) = 2.2 \pm 0.6$  mag. Instead, by comparing  $\text{Pa}\beta$  with the broad component of  $\text{H}\alpha$ , and assuming an intrinsic  $\text{Pa}\beta/\text{H}\alpha = 0.052$ , we derive  $A_V(\text{BLR}) = 3.5 \pm 0.4$  mag. However, the latter value is less reliable both because radiation transport and collisional excitation might affect the intrinsic  $\text{Pa}\beta/\text{H}\alpha$  ratio in the BLR, and because problems of intercalibration between the optical and the infrared spectra might affect the observed value. The extinction toward the NLR can be derived by the narrow components of  $\text{Pa}\beta$  and  $\text{H}\alpha$ : we obtain  $A_V(\text{NLR}) = 2.0 \pm 0.6$  mag<sup>5</sup>, consistent with what obtained for the broad line region. This finding suggests that both BLR and NLR are absorbed by the same (large scale) medium, possibly the 100 pc scale dust lane observed in the images.

The optical-infrared absorption towards the BLR is lower than that expected from the  $N_H$  measured from the X-ray spectrum. By assuming a Galactic gas-to-dust ratio we find  $A_V(X) = 4.5 \times 10^{-22} N_H(\text{cm}^{-2}) = 4.5$ . As suggested by Granato et al. (1997), this mismatch between optical and X-ray absorption might indicate the presence of a dust-free region in the X-ray absorber. Alternatively, the obscuring gas might be characterized by a gas-to-dust ratio lower than Galactic or the average dust grain size might be larger than in the interstellar Galactic medium, thus making the extinction curve flatter (Laor and Draine 1993).

## 5. Conclusions

In this paper we have shown that an AGN has revived in the center of NGC 2992. The spectral continuum detected both in SAX1 (1997) and SAX2 (1998) can be described with a power law with  $\Gamma = 1.7$  absorbed by  $N_H = 10^{22} \text{cm}^{-2}$ , which is consistent with the mean spectrum of NGC 2992 observed in the past. A prominent iron  $\text{K}\alpha$  line is also detected in both the data sets. The SAX1 observation is located between the ASCA and the SAX2 observations (which correspond to the lowest and highest states of the source, respectively), and seems to have caught the source during the rebuilding phase of the accretion disc. From the properties of the iron line detected

<sup>5</sup> Ward et al. (1980) obtained a value of  $A_V(\text{NLR}) = 4.2$  from the narrow lines  $\text{H}\alpha/\text{H}\beta$  Balmer decrement. Part to the difference with our result is to ascribe to a different extinction curve and an adopted intrinsic ratio lower than currently assumed for the narrow line region of AGNs (i.e. 2.8 instead of 3.0); if we use their narrow line Balmer decrement with our extinction curve and the “correct” intrinsic ratio we obtain  $A_V(\text{NLR}) = 3.7$ . Moreover the  $\text{H}\beta$  line is probably affected by the corresponding stellar  $\text{H}\beta$  in absorption (Ward et al. spectrum shows evidence for stellar features) that artificially increases the Balmer decrement. Finally the limited spectral resolution might have resulted in problems with the emission lines deblending.

<sup>4</sup> This is not necessarily the maximum near-IR emission that can be achieved by the nucleus, since in 1988 the burst was temporary and did not last very long and, therefore, probably not all of the hot dust emitting region was completely formed.

in SAX1, the forming disc appears to be constituted by gas which is still far from the central black hole and is highly ionized, possibly because of its low density. During the SAX2 observation the disc appears to be almost completed and the iron line properties fit into the standard (cold) disc models.

We also presented the results of optical and near-IR followup observations obtained 1.5 months after the detection of the X-ray burst. The optical and near-IR hydrogen lines are characterized by prominent broad components, with intensities comparable to those observed in the former active phase prior to 1979. The near-IR images and the near-IR spectrum also show evidence for hot dust emission in the H and K bands. However, at the time of the observations the K and H band nuclear emission was still not as high as observed in a previous IR burst, suggesting that hot dust region was still in the process of forming.

*Acknowledgements.* We thank Chris Lidman, the NTT and SOFI staff for performing the near infrared and optical observations. We thank Roberto Della Ceca for helpful comments. We are grateful to M. Allen and M. Dopita for providing their optical spectrum of the nucleus of NGC 2992. The referee is thanked for his comments. This work was partly supported by the Italian Space Agency (ASI) under grant ARS-98-116/22 and by the Italian Ministry for University and Research (MURST) under grant Cofin98-02-32.

## References

- Allen M.G., Dopita M.A., Tsvetanov Z.I., Sutherland R.S., 1999, *ApJ* 511, 686
- Antonucci R.R.J., Miller J.S., 1985, *ApJ* 297, 621
- Boella G., Butler R.C., Perola G.C., Piro L., Scarsi L., Bleeker J., 1997a, *A&AS* 122, 299
- Boella G., Chiappetti L., Conti G. et al., 1997b, *A&AS* 122, 327
- Cappi M., Mihara, T., Matsuoka, M., Brinkmann, W., Prieto, M.A., Palumbo, G.G.C., 1996, *ApJ*, 456, 141
- Durret F., 1990, *A&A* 229, 351
- Fabian A.C., Rees M.J., Stella L., White N.E., 1989, *MNRAS* 238, 729
- Frontera F., Costa E., Dal Fiume D. et al., 1997, *A&AS* 122, 357
- George I.M., Fabian A.C., 1991, *MNRAS* 249, 352
- Ghisellini G., Haardt F., Matt G., 1994, *MNRAS* 267, 743
- Glass I.S., 1997, *MNRAS* 292, L50
- Goodrich R.W., Veilleux S., Hill G.J., 1994, *ApJ* 422, 521
- Granato G.L., Danese L., Franceschini A., 1997, *ApJ* 486, 147
- Guainazzi M., Nicastro F., Fiore F., et al., 1998, *MNRAS* 301, L1
- Guainazzi M., Perola G.C., Matt G. et al., 1999, *A&A* 346, 407
- Haardt F., Maraschi L., *ApJ* 380, L51
- Haardt F., Fossati G., Grandi P. et al., 1998, *A&A* 340, 35
- Hamuy M., Walker A.R., Suntzeff N.B., Gigoux P., Heathcote S.R., Phillips M.M., 1992, *PASP* 104, 533
- Hamuy M., Suntzeff N.B., Heathcote S.R., Walker A.R., Gigoux P., Phillips M.M., 1994, *PASP* 106, 566
- Krolik J.H., Kallman T.R., 1987, *ApJ* 320, L5
- Laor A., 1991, *ApJ* 376, 90
- Laor A., Draine B.T., 1993, *ApJ* 402, 441
- Magdziarz P., Zdziarski A.A., 1995, *MNRAS* 273, 837
- Maiolino R., Rieke G.H., Rieke M.J., 1996, *AJ* 111, 537
- Maiolino R., Krabbe A., Thatte N., Genzel R., 1998, *ApJ* 493, 650
- Malaguti G., Bassani L., Cappi M. et al., 1999, *A&A* 342, L41
- Manzo G., Giarrusso S., Santangelo A. et al., 1997, *A&AS* 122, 341
- Matt G., Perola G.C., Piro L., Stella L., 1992, *A&A* 257, 63
- Matt G., Fabian A.C., Ross R.R., 1993, *MNRAS* 262, 179
- Matt G., Brandt W.N., Fabian A.C., 1996, *MNRAS* 280, 823
- Matt G., Guainazzi M., Frontera F. et al., 1997, *A&A* 325, L13
- Mulchaey J.S., Koratkar A., Ward M.J., Wilson A.S., Whittle M., Antonucci R.R.J., Kinney A., Hurt T., 1994, *ApJ* 436, 586
- Mushotzky R.F., 1982, *ApJ* 256, 92
- Nandra K., Pounds K.A., 1994, *MNRAS* 268, 405
- Nandra K., George I.M., Mushotzky R.F., Turner T.J., Yaqoob T., 1997a, *ApJ* 476, 70
- Nandra K., George I.M., Mushotzky R.F., Turner T.J., Yaqoob T., 1997b, *ApJ* 477, 602
- Narayan R., Mahadevan R., Quataert E., 1998, to appear in: Abramowicz M.A., Bjornsson G., Pringle J.E. (eds.) *The Theory of Black Hole Accretion Discs* [astro-ph/9803141]
- Netzer H., 1990, in: Courvoisier R.J.L., Mayor M. (eds.) *Active Galactic Nuclei*. Springer, Berlin, p. 57
- Netzer H., Laor A., 1993, *ApJ* 404, L51
- Oliva E., Origlia L., 1992, *A&A* 254, 466
- Oliva E., Origlia L., Kotilainen J.K., Moorwood A.F.M., 1995, *A&A* 301, 550
- Oliva E., Maiolino R., Origlia L., Moorwood A.F.M., 1999, *A&A* in press
- Parmar A.N., Martin D.D.E., Bavdaz M. et al., 1997, *A&AS* 122, 309
- Ptak A.F., Yaqoob T., Mushotzky R.F., Serlemitsos P.J., Griffiths R., 1998, *ApJ* 501, L37
- Persson S.E., Murphy D.C., Krzeminski W., Roth M., Rieke M.J., 1998, *AJ* 116, 2475
- Rieke G.H., Lebofsky M.J., 1985, *ApJ* 288, 618
- Rix H.-W., Carleton N.P., Rieke G., Rieke M., 1990, *ApJ* 363, 480
- Risaliti G., Maiolino R., Bassani L., 1999, *A&A* in press
- Shuder J.M., 1980, *ApJ* 240, 32
- Thatte N., Quirrenbach A., Genzel R., Maiolino R., Tecza M., 1997, *ApJ* 490, 238
- Turner T.J., George I.M., Nandra K., Mushotzky R.F., 1997, *ApJS* 113, 23
- Ueno S., Mushotzky R.F., Koyama K., Iwasawa K., Awaki H., Hayashi I., 1994, *PASJ* 46, L71
- Veron P., Lindblad P.O., Zuiderwijk E.J., Adam G., Veron M.P., 1980, *A&A* 87, 245
- Ward M., Penston M.V., Blades J.C., Turtle A.J., 1980, *MNRAS* 193, 563
- Weaver K.A., Arnaud K.A., Mushotzky R.F., 1995, *ApJ* 447, 121
- Weaver K.A., Nousek J., Yaqoob T., Mushotzky R.F., Makino F., Otani C., 1996, *ApJ* 458, 160
- Winkler H., 1992, *MNRAS* 257, 677

### Appendix A: List of line fluxes

In Tab. A1 we list the lines detected in our optical and near-IR spectra. In the case of permitted lines, the flux given in the last column gives the total line flux, i.e. both broad and narrow components. In the case of blending the line fluxes were obtained by means of a multiple Gaussian fit. In cases for which the blending is excessive to allow a deconvolution we give the total flux of the blend.

We could not derive a flux for the HeI  $\lambda 6678$  since it is severely blended with the H $\alpha$  wings and with the [SII] doublet, resulting in a plateau between the two groups of lines. Some uncertainties exist for the identification of the line at 13305 Å : it could either be fluorescence OI  $\lambda 13170$ Å or [FeII]  $\lambda 13205$ Å. We favor the latter identification both because it matches much better the observed wavelength and because the observed flux is in excellent agreement with that expected from [FeII] $\lambda 12567$ Å (the observed ratio between the two lines is 3.26, while the theoretical value is 3.75). The absence of OI  $\lambda 13170$ Å strongly suggests that the OI  $\lambda 11290$ Å line is produced by *Ly $\beta$  fluorescence* and *not* by continuum fluorescence (in the latter case both OI lines should have nearly the same intensity). *Ly $\beta$  fluorescence* is also supported by the lack of OI lines at 7002 Å and 7255 Å . We could not find any identification for the line detected at 7431 Å , possibly this might be an instrumental artifact.

**Table A1.** Optical and near-infrared emission lines detected in our spectra.

Identification	$\lambda_{\text{obs}}^a$	Flux <sup>b</sup>
[OI] $\lambda 6300$	6349.5	5.2
[OI] $\lambda 6364$	6413.6	1.74
[FeX] $\lambda 6374$	6421.	0.6 <sup>c</sup>
[NII] $\lambda 6548$	6597.8	8.0
H $\alpha$ $\lambda 6563$	6612.	195.
[NII] $\lambda 6583$	6633.5	24.
HeI $\lambda 6678$	6728.	— <sup>f</sup>
[SII] $\lambda 6716$	6767.	11.1
[SII] $\lambda 6731$	6781.	11.9
HeI $\lambda 7065$	7110.	7.8
[ArIII] $\lambda 7136$	7188.	2.7
[OII] $\lambda \lambda 7318-7330$	7379.	3.3
unident.	7431.	0.95
[ArIII] $\lambda 7751$	7810.	0.34
[FeXI] $\lambda 7891$	7948.	0.12
[SIII] $\lambda 9531$	9605.1	31.
Pa $\epsilon$ $\lambda 9546$	9619.5	26. <sup>c</sup>
[Cl] $\lambda 9850$	9930.	2.2 <sup>c</sup>
[SVIII] $\lambda 9912$	9990.	2.2 <sup>c</sup>
Pa $\delta$ $\lambda 10049$	10126.	26.5
HeII $\lambda 10123$	10201.	3.7 <sup>c</sup>
[SII] $\lambda 10286$	10365.	2.2 <sup>c</sup>
[SII] $\lambda \lambda 10320+10336$	10408.	2.9 <sup>c</sup>
HeI $\lambda 10830$	10917.	123.6
Pa $\gamma$ $\lambda 10938$	11023.	37. <sup>c</sup>
OI $\lambda 11290$	11383.	6.9 <sup>d</sup>
[SIX] $\lambda 12524$	12622	1.8 <sup>c</sup>
[FeII] $\lambda 12567$	12669	7.5
Pa $\beta$ $\lambda 12818$	12920	51.
[FeII] $\lambda 13205$	13305	2.9
Br13 $\lambda 16109$	16238	2.8
[FeII] $\lambda 16435^e$	16570	5.9
Br11 $\lambda 16806$	16944	5.6
Br10 $\lambda 17362$	17534	7.3
Pa $\alpha$ $\lambda 18751$	18895	88. <sup>d</sup>
H2(1-0)S(3) $\lambda 19576$	19725	5. <sup>c,d</sup>
[SIV] $\lambda 19635$	19793	4. <sup>c,d</sup>
H2(1-0)S(2) $\lambda 20332$	20499	2.4 <sup>d</sup>
HeI $\lambda 20581$	20743	7.
H2(1-0)S(1) $\lambda 21218$	21388	2.5
Br $\gamma$ $\lambda 21655$	21837	11.6

<sup>a</sup> Observed wavelength in Å .

<sup>b</sup> Integrated flux in units of  $10^{-15}$ erg cm<sup>-2</sup> s<sup>-1</sup>. For lines with broad components this column gives the total flux (narrow+broad).

<sup>c</sup> Flux poorly determined (30–50% uncertainty) due to blending with other lines.

<sup>d</sup> Flux poorly determined (30–50% uncertainty) because the line is in a region of bad atmospheric transmission.

<sup>e</sup> We assume that the narrow line observed at 1.65  $\mu\text{m}$  is dominated by the [FeII] line, with little contribution from Br12 (that is much broader).

<sup>f</sup> We could not derive a flux for this line due to its sever blending with H $\alpha$  wings and the [SII] doublet.